Electrorefining of U-Pu-Zr-alloy fuel onto solid aluminium cathodes in molten LiCl-KCl

By P. Souček[1], L. Cassayre[2], R. Malmbeck[1,*], E. Mendes[1], R. Jardin[1] and J.-P. Glatz[1]

[1] European Commission, JRC, Institute for Transuranium Elements (ITU), Postfach 2340, 76125 Karlsruhe, Germany
[2] Laboratoire de Génie Chimique (LGC), Université Paul Sabatier, UMR CNRS 5503, 118 route de Narbonne, 31062 Toulouse Cedex 04, France

(Received July 12, 2007; accepted in revised form September 6, 2007)

Pyrochemical separation / Electrorefining / Actinides / Alloy formation / LiCl-KCl eutectic

Summary. An electrorefining process in molten chloride salts using solid aluminium cathodes is being developed at ITU to recover actinides (An) from the spent nuclear fuel. The maximum possible loading of aluminium electrodes with actinides was investigated during the electrorefining of U-Pu-Zr alloy in a LiCl-KCl eutectic at 450 °C. Two different electrolytic techniques were applied during the experiment and almost 6000 C has been passed, corresponding to 3.7 g of deposited actinides. A very high capacity of aluminium to retain actinides has been proven as the average Al : An mass ratio was 1 : 1.58 for galvanostatic and 1 : 2.25 for potentiostatic mode. The obtained deposits were characterized by XRD and SEM-EDX analysis and alloys composed of (U,Pu)Al_3 were detected. The influence of zirconium co-oxidation during the process was also investigated and the presence of dissolved Zr ions in the melt yielded a significant deterioration of the quality of the deposit.

1. Introduction

Partitioning and transmutation technologies are investigated worldwide in order to minimize the long term radiotoxicity of the highly radioactive spent nuclear fuel produced at present during operation of the conventional nuclear reactors. The development of efficient partitioning techniques is also a key point for future reactor systems, where the application of an integrated advanced nuclear fuel cycle is considered [1–3]. Pyrochemical reprocessing is an option for the management of all actinides (An) in advanced fuels or minor actinides (MA = Am, Cm) in transmutation targets which might not be suitable for reprocessing using aqueous-based processes.

Electrorefining and molten salt/liquid metal reductive extraction are the most developed pyrochemical separation techniques. In the electrorefining process developed in Argonne National Laboratory, uranium in metallic alloy fuel is recovered onto inert solid steel cathodes [4] and the process has been further developed to recover also Pu and MA in liquid Cd cathodes [5, 6]. The use of reactive electrodes is very advantageous for the recovery of actinides, as the actinide metals are stabilized by the formation of alloys with the cathode material. According to the known activity coefficients of Pu, U and Ce in different reactive metals, aluminium has been identified as the electrode material enabling the highest separation factors of actinides from lanthanides (Ln) [7]. This has led to the development of a process based on the separation of actinides by reductive extraction into molten Al pool [8].

In ITU, an electrorefining process in molten chloride salt using solid aluminium cathodes is being developed [9]. In this process, actinides are recovered from a metallic An-Zr alloy fuel in the form of An-Al alloys. A very high selectivity of the process for recovery of An from Ln has been already shown as well as the capability of solid aluminium electrodes to form stable An-Al alloys using Al rods, foils [9] and a foam [10] as the cathodes. In addition, a large-surface aluminium electrode has been used to study the maximum amount of actinides that can be collected on a single electrode by a constant current electrolysis [11].

In this paper, this issue has been further investigated by U and Pu electrodeposition applying potentiostatic and galvanostatic electrolytic techniques and using Al plate cathodes of different dimensions with the objective to reach as high An loading as possible. The experiment was carried out with U-Pu-Zr alloy (71-19-10 wt. %) anodes and a relatively high concentration of actinides in the bath (up to 10 wt. %). Gadolinium chloride was also introduced in the bath at a concentration of 1.6 wt. % to verify the selectivity of the process compared to lanthanides. The electrodes deposits were characterised by γ-spectroscopy, SEM-EDX analysis and XRD.

2. Experimental

All experiments and storage and handling of chemicals were carried out in a glovebox under purified Ar atmosphere (< 5 ppm of water and oxygen). The detailed description of the technique is described in reference [12]. Cyclic voltammetry (CV) measurements were carried out using a three-electrode setup and a PAR 273 potentiostat with EG&G M270 electrochemical software. The working electrode was prepared using a metallic wire ($d = 1$ mm) and inserted approximately 5 mm into the bath, while a Mo wire bent into the shape of a spiral served as the auxiliary electrode.

*Author for correspondence
(E-mail: rikard.malmbeck@ec.europa.eu).

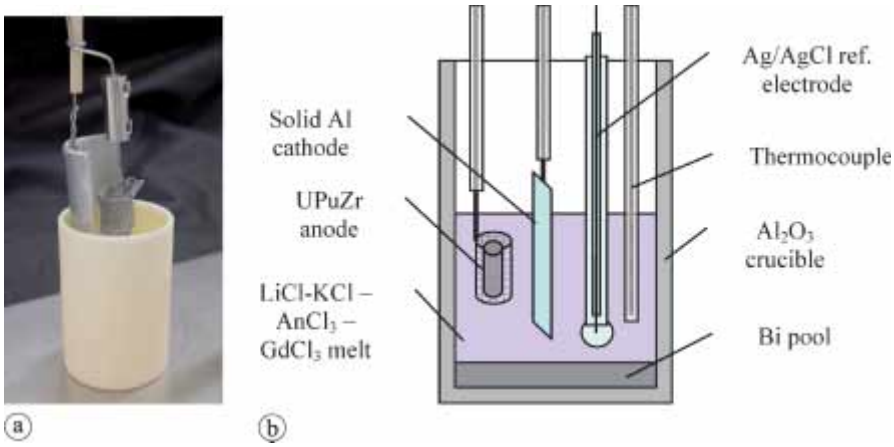

Fig. 1. Picture of anodic basket, cathode and crucible before start of the experiment (**a**) and scheme of experimental set-up (**b**).

The reference electrode used was an Ag/LiCl-KCl-AgCl (1 wt. %) prepared in a Pyrex glass tube and potential values mentioned in this work refer to this reference potential.

During the electrorefining experiments, an aluminium plate was used as a cathode and a tantalum basket containing the U-Pu-Zr alloy (ITU stock material, 71-19-10 wt. % respectively) was connected as an anode. All cathodes were made either from 0.5 mm or 2.0 mm thick aluminium plate and the dimensions of the immersed part varied from 5×20 to 40×20 mm^2. The active part of the cathode surface area was determined after each experiment by measuring the immersion depth of the electrode. Both anodic and cathodic potentials were simultaneously monitored during the electrolysis using the above-described Ag/AgCl reference electrode. A specially-prepared combination of two multimeters with a laboratory power supply served both for control of the process and for data acquisition. The scheme of the experimental set-up used during electrorefining experiments and a picture of the anodic basket, cathode and crucible are shown in Fig. 1.

A bath consisting of U^{3+}, Pu^{3+} and Gd^{3+} ions dissolved in the LiCl-KCl eutectic mixture (Aldrich 99.99%) was prepared by oxidation of a piece of the U-Pu-Zr metallic alloy dipped into the melt in a tantalum basket. The preparative oxidation was performed by addition of $BiCl_3$ according to reaction (1).

$$\mathrm{An}^0_{\text{U-Pu-Zr}} + \mathrm{Bi}^{3+}_{\text{salt-phase}} \rightleftharpoons \mathrm{An}^{3+}_{\text{salt-phase}} + \mathrm{Bi}^0 \quad (\mathrm{An} = \mathrm{U}, \mathrm{Pu})\,. \tag{1}$$

The reduced Bi metal was collected in a Bi pool at the bottom of the Al_2O_3 crucible. $GdCl_3$ (Aldrich 99.99%) was used as received from the producer without any additional treatment. The initial concentrations in the bath were analysed to be 1.84 wt. % U, 2.08 wt. % Pu and 1.30 wt. % Gd. By further oxidation, the actinides content was increased during the experiment up to 6.03 wt. % U and 4.48 wt. % Pu, *i.e.* in total more than 10 wt. % actinides in the salt. The oxidation reaction was followed by CV measured on an inert tungsten electrode. The chemical composition of the salt was monitored by ICP-MS analysis of regularly-taken salt samples dissolved in 1 M nitric acid. After the electrorefining, the adhered salt on the electrodes was removed by vacuum distillation and/or by washing in ethanol. SEM/EDX and XRD was used for some surface analysis and the deposit composition was investigated by γ spectrometry [13].

3. Results and discussion

3.1 Cyclic voltammetry

Cyclic voltammetry measurements on an inert W working electrode were used to monitor the quality of the bath during the complete experiment. A voltammogram of the bath containing dissolved U (3.17 wt. %), Pu (1.18 wt. %), Gd (1.66 wt. %) and Zr (0.32 wt. %, oxidised during the course of the experiment) is shown in Fig. 2. The first cathodic wave I_c is attributed to the soluble–soluble transition associated with U^{4+}/U^{3+} transition at -0.25 V [14]. The following peaks II_c–V_c represent the reduction of Zr [15], U [14], Pu [16] and Gd [17] ions to metals in reaction $M^{3+} + 3e^- \rightarrow M$, respectively.

On a reactive aluminium electrode, the deposition potentials of both actinides and lanthanides are shifted to more positive values due to the formation of alloys with the electrode material. The values of the deposition potentials on Al have been published for U [11], Pu [10] and Gd [18, 19] (see Table 1). Due to the different concentrations of AgCl in the

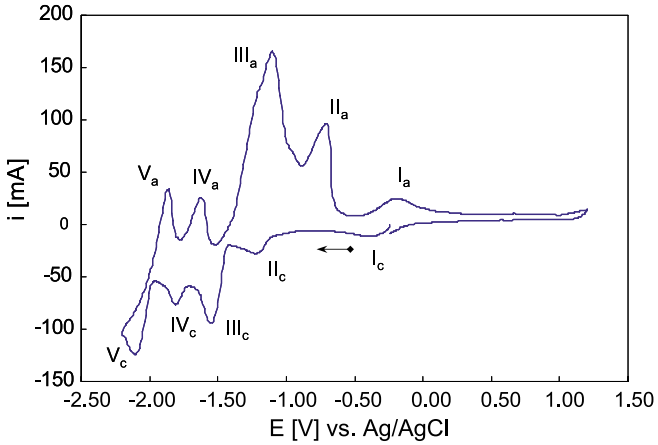

Fig. 2. Cyclic voltammogram of the bath containing dissolved U (3.17 wt. %), Pu (1.18 wt. %), Gd (1.66 wt. %) and Zr (0.32 wt. %) measured on W electrode, 100 mV s^{-1}, 460 °C. Cyclic voltammogram of the bath containing dissolved U (3.17 wt. %), Pu (1.18 wt. %), Gd (1.66 wt. %) and Zr (0.32 wt. %) measured on W electrode, 100 mV s^{-1}, 460 °C.

Table 1. Measured deposition potentials of U, Pu and Gd on solid Al in molten LiCl-KCl.

Reduced ions	Temperature [K]	Concentration in the salt [wt. %]	Dep. potential [E *vs.* Ag/AgCl]	Ref.
U^{3+}	733	1.50	−1.05	[11]
Pu^{3+}	733	1.25	−1.18	[10]
Gd^{3+}	723	1.58–2.64[a]	−1.44	[18]
Gd^{3+}	733	1.58	−1.41	[19]

a: Exact concentration used for the measurement with solid Al electrode is not specified in the reference.

used reference electrodes, the potentials were recalculated to the scale of Ag/AgCl (1 wt. %) reference electrode. The difference in the deposition potentials between Pu and Gd onto Al is 230 mV, which is enough to provide a selective deposition of actinides.

3.2 Electrorefining of U-Pu-Zr alloy

Galvanostatic and potentiostatic electrolysis were used to examine the maximum possible loading of the solid Al electrodes. In the galvanostatic mode, the maximum current was reached after applying a stepwise current increase while maintaining both cathodic and anodic potentials within the selected limits. The cathodic cut-off potential was set to a value of −1.25 V which ensures conditions for a selective grouped separation of An from Ln [10, 11]. A potential of −1.00 V was used as the anode cut-off potential to avoid oxidation of Zr from the U-Pu-Zr alloy [20]. For all runs under potentiostatic conditions, a cathode potential of −1.25 V was applied. The electrolysis was terminated when the current became too low or if the expected loading of the cathode was achieved.

In total 5 runs were carried out (see Table 2). The expected electrode reactions were anodic oxidation of actinides from the alloy and their reduction on the cathode forming An-Al alloys according to the following reaction schemes:

$$\text{Anodic side: } M_x{}^0Zr_y \rightarrow M^{3+} + 3e^- + M_{x-1}{}^0Zr_y \quad (2)$$

$$\text{Cathodic side: } M^{3+} + 3e^- + zAl \rightarrow M^0Al_z \quad (M = U, Pu)\,. \quad (3)$$

In addition to the two galvanostatic and two potentiostatic runs, one experiment was performed without applying an anodic cut-off potential to evaluate the influence of oxidation and co-deposition of Zr on the quality of the deposit (run 2). Because of a poor adhesion of the deposit, only qualitative evaluation is available for this run (see Sect. 3.4).

3.2.1 Galvanostatic electrolysis

Galvanostatic experiments were carried out using large area Al electrodes made from plates either 0.5 or 2.0 mm thick. The thinner plates were used to examine the capacity of an Al electrode to retain actinides (runs 1 and 3). For these two experiments, an excess of U-Pu-Zr alloy was introduced as anodic material to avoid Zr co-dissolution during the electrolyses. The anodic potential varied between −1.30 and −1.00 V, which corresponds to a congruent oxidation of the actinides from the U-Pu-Zr alloy.

Selective reduction of uranium and plutonium forming a U-Pu-Al surface alloy occurred at the cathode and the potential showed a decreasing trend, starting from −1.05 V and in the end reaching the minimum value of −1.25 V. With the build up of the An-Al surface alloy layer, the cathodic reaction is more and more limited by diffusion of the reduced elements forming the surface alloy layer, *i.e.* U, Pu and Al. The record of potentials and current for the galvanostatic electrolysis in run 3 is presented in Fig. 3.

The thicker plate was used for the measurement without anodic limitation and a stoichiometric amount of the alloy was added to the anodic basket (run 2). During the electrolysis co-oxidation of zirconium together with the actinides occurred at the anode, which was evidenced by a positive shift in anodic potential from −1.30 V to −0.70 V. Moreover, Zr ions released from the anode were also reduced onto the aluminium cathode together with the actinides, as the deposition potential of Zr is more positive than that of the actinides.

3.2.2 Potentiostatic electrolysis

Two potentiostatic electrolyses were carried out with small area electrodes made from plates of 0.5 and 2.0 mm thickness (runs 4 and 5). The aim was to examine the Al electrode capacity to alloy actinides and consequently an excess of U-Pu-Zr alloy was used as anodic material. The cathodic potential was kept constant at −1.25 V in both runs to ensure a selective deposition of actinides.

The record of anodic potential development and current for a typical potentiostatic electrolysis (run 5) is shown in Fig. 4. In this case, the current gradually decreased from

Table 2. Runs carried out during U-Pu-Zr electrorefining experiment.

Run	Technique	Cathode			Treatment	Analysis		
		Mass [g]	Thickness [mm]	Surface [cm^2]	Vacuum distillation	γ-spectroscopy	SEM-EDX	XRD
1	GE + L	0.61	0.5	9.3	yes	yes	yes	yes
2	GE	2.43	2.0	10.2	no	no	yes	yes
3	GE + L	0.54	0.5	8.3	yes	yes	no	no
4	PE	0.27	2.0	1.5	no	yes	no	no
5	PE	0.23	0.5	3.6	no	yes	no	no

GE (+L) = Galvanostatic electrolysis (applying limiting cut-off potentials); PE = potentiostatic electrolysis.

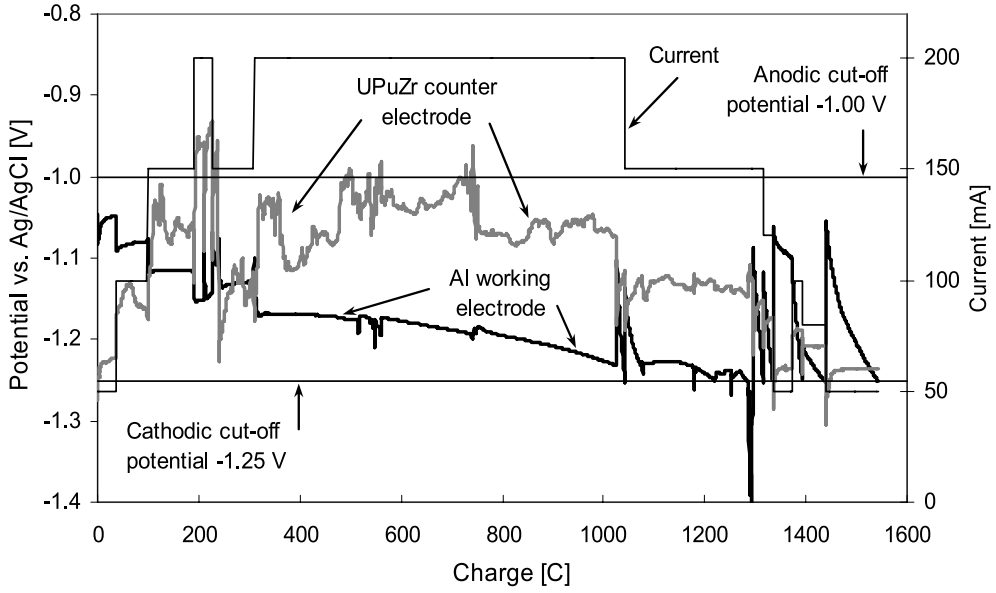

Fig. 3. Evolution of cathodic and anodic potentials during the galvanostatic electrolysis using both cut-off potentials (Run 3).

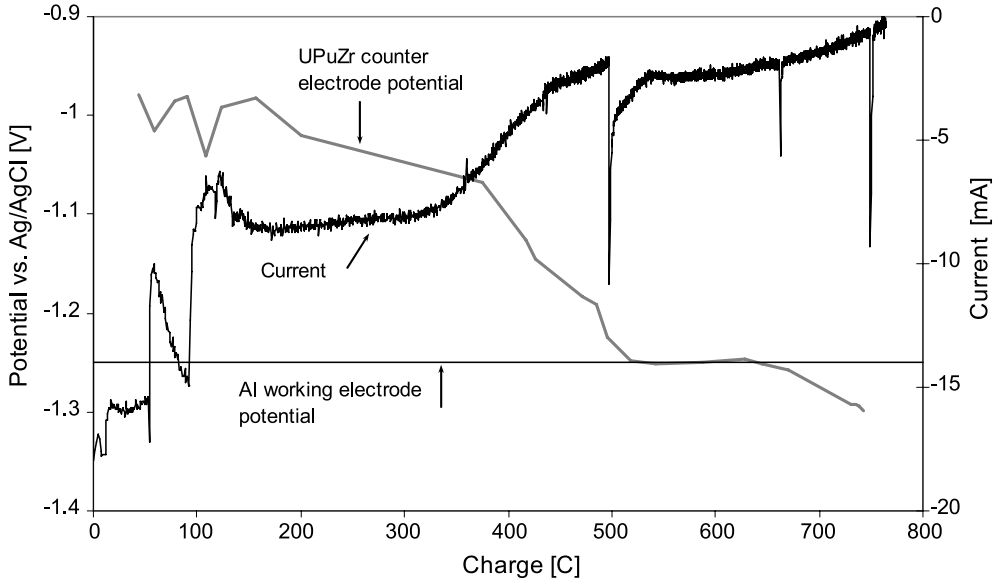

Fig. 4. Evolution of anodic potential and current during the potentiostatic electrolysis (run 5) at $E = -1.25$ V *vs.* Ag/AgCl.

-20 mA to almost 0 as a result of the increasing thickness of the U-Pu-Al alloy. Due to the decrease of the current, the anodic potential symmetrically dropped from -1.0 V up to -1.3 V.

3.3 Evaluation of the Al electrodes capacity to load actinides

After the electrodeposition, the electrodes were left for some time just above the bath at 450 °C in order to let the adhered salt drop down. The estimated mass of adhered salt was in the order of 0.2 g. In two cases (run 1 and 3), a vacuum distillation was used for removal of the salt that remained on the electrode surface. The efficiency of the distillation (performed at 500 °C) turned out to be quite low and at most only 50% of the salt was removed.

A quantitative Pu assay was performed by gamma spectrometry in a far-field counting geometry (sample-to-detector distance = 19 cm) relative to a Pu reference sample of similar Pu isotopic composition and known Pu element content. The relative accuracy of this kind of Pu assay is estimated to be 5%. Separate gamma measurements with close sample-to-detector distances were performed for the determination of the Pu/U ratio using gamma rays from ^{239}Pu and ^{235}U, combined with the known isotopic composition of Pu and U for the calculation of the Pu/U weight ratio. The relative uncertainty of the measured Pu/U weight ratio ranges between 1.7 and 2.5%. The results are summarised in Table 3 (quoted uncertainties at ±1-sigma).

Table 3. Gamma spectroscopy analysis of U and Pu content in the electrodes' deposits.

Run	Pu content (mg)	U/Pu Weight ratio	U content (mg)	Sum (Pu + U) (mg)
1	84.0 ± 4.2	10.09 ± 0.17	849 ± 44	933
3	47.1 ± 2.4	18.07 ± 0.30	852 ± 45	899
4	51.0 ± 2.6	11.35 ± 0.19	579 ± 30	630
5	67.7 ± 3.4	6.37 ± 0.16	431 ± 24	499

Table 4. Evaluation of results achieved during U-Pu-Zr electrorefining experiments.

Run	Charge	Mass	Deposit weight [mg]		Current	An	Weight
	[C]	Al [g]	Theoretical	Analysed	efficiency [%]	wt. %	ratio Al/An
1	1423	0.61	1171	933	79.7	59.9	1 : 1.49
3	1527	0.54	1256	899	71.6	62.5	1 : 1.67
4	773	0.27	632	630	99.7	70.0	1 : 2.33
5	766	0.23	637	499	78.3	68.5	1 : 2.17

The evaluation of the loading of the electrodes with actinides is given in Table 4. The weight percent ratio of An in the Al cathode was calculated according to Eq. (4):

$$\text{An wt. \% in Al} = \frac{m_{\text{An}}}{m_{\text{An}} + m_{\text{Al}}} . \quad (4)$$

The mass of actinides m_{An} resulting from gamma spectroscopy measurements was used for the calculation and the relevant aluminium mass was derived from the measured immersed depths of each electrode. The theoretical mass of the deposit was calculated assuming 100% faradic yield, thus the charge passed during the experiment was converted to a mass of actinides (according to the U/Pu ratio obtained from the gamma measurement) collected on the cathode.

If $AnAl_3$ alloy is assumed as the main constituent of the formed deposit, the maximum possible loading is 2.94 g of An in 1 g of Al, which corresponds to 74.7 wt. % An in Al. The highest An content in Al was achieved for potentiostatic electrolysis, with 2.33 g of An loaded into 1 g of Al (70.0 wt. % An in Al). This is 94 % of the maximum Al capacity. The average value was 2.25 g of An, *i.e.* 69.3 wt. % An in Al. In galvanostatic electrolyses, the average loading achieved was somewhat lower, 1.58 g of An in 1 g of Al (61.2 wt. % An in Al). Nevertheless, it still confirms a high capacity of Al to take up actinides

The diffusion of An and Al through the An-Al alloy surface deposit seems likely to be the most important factor for this process. As the diffusion rate increases with temperature, then actinide-richer and possibly thicker alloy layers could be expected at higher temperatures. More detailed studies will be necessary to correctly evaluate the dependency of the maximum actinide loading of aluminium cathodes during electrorefining on the applied temperature and the thickness of the cathodes.

3.4 Characterization of the alloys

Electrodes from run 1 and 2 were further characterized by SEM-EDX analysis and XRD. The aim was to evaluate the thickness, the structure and the composition of the formed An-Al alloys (run 1) and to assess the influence of Zr co-deposition on the quality of the deposit (run 2). From each electrode a piece was cut, embedded in epoxy resin and surface-polished for SEM analyses. From the remaining cathode some deposit was scraped off, well ground and embedded in epoxy resin and slightly polished for precise X-ray powder diffraction analysis.

3.4.1 Galvanostatic electrolysis applying both potential limits

The electrode from run 1 was selected to be characterized by SEM-EDX analysis. SEM micrographs and results of EDX analysis are shown in Figs. 5 and 6. A uniformly thick and porous surface deposit is well visible on the micrograph shown in Fig. 5a. At some places, almost all aluminium has reacted, as shown in Fig. 5b, which corresponds well to the above-calculated An/Al weight ratio of 1.5. The maximum thickness of the deposit with no Al metal remaining was measured as 1.2 mm (see arrows in Fig. 5b), compared to 0.5 mm initially.

An analysis of the deposit was performed using EDX at 21 spots selected at various heights of the electrode with different thicknesses of deposit. Composition profiles from the middle towards the surface of the electrode were compiled for U, Pu, Al, Cl and Gd. As expected, Gd was not detected in the deposit. Cl was found in the porous parts, which indicates the presence of salt inclusions. The molar ratio Al/(U + Pu) is plotted in Fig. 6 as function of the distance from the centre of the electrode. The average Al/(U + Pu) ratio was determined to be 3.01. Thus the deposit is most

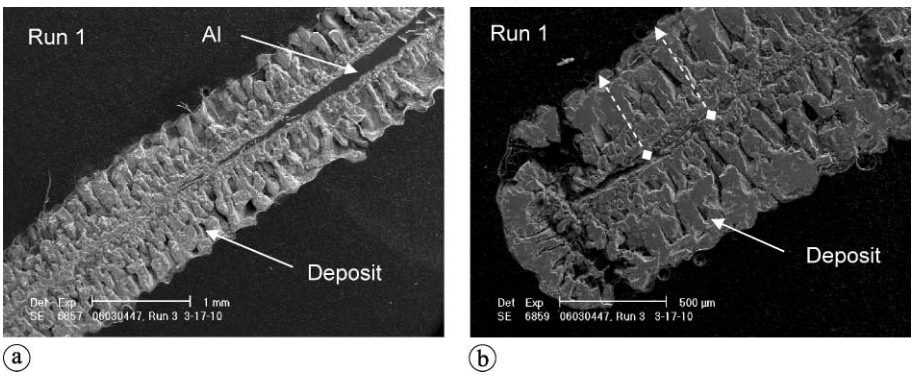

(a) (b)

Fig. 5. SEM micrographs of the cross-sections of electrode from run 1.

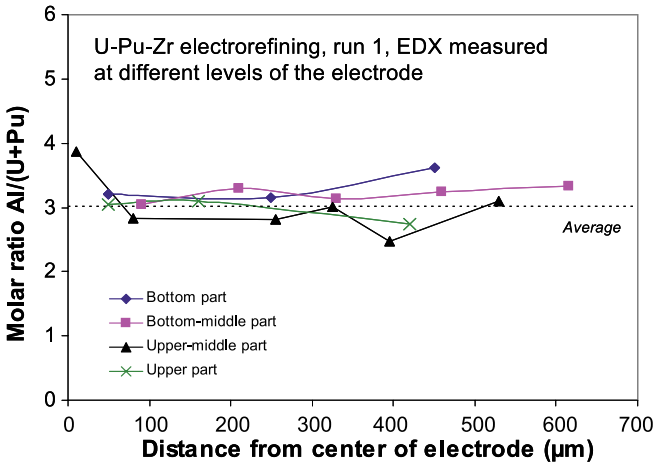

Fig. 6. SEM-EDX determination of the Al/(U + Pu) molar ratio *vs.* the distance from the electrode surface (run 1).

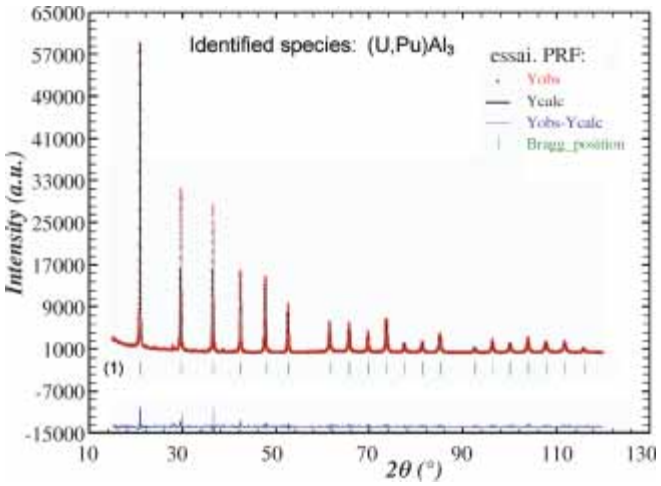

Fig. 7. XRD pattern of the deposit from run 1 (Symbols = observed points, solid line above = calculated profile, solid line below = difference between observed and calculated profiles, ticks below the peaks = $2\theta_{hkl}$ Bragg positions: (1) UAl_3).

probably composed of a (U,Pu)Al_3 alloy. The values for the U/Pu molar ratio were scattered, with a U/Pu ratio comprised between 4 and 10. The average value was U/Pu = 7.0, which is somewhat lower than the ratio determined by gamma spectroscopy (10.1).

The XRD pattern of the deposit was indexed on the basis of a cubic ($a = 4.2652(1)$ Å) unit cell corresponding to (U,Pu)Al_3 alloy. This result is in a very good agreement with the EDX determination of the Al/(U + Pu) molar ratio (average value 3.01). Although the cell parameters for UAl_3 and $PuAl_3$ are very similar (4.266 Å and 4.264 Å, respectively [21, 22]), the measured spectrum indicates the formation of a (U,Pu)Al_3 solid solution, as no splitting of diffraction peaks was observed. The XRD pattern is shown in Fig. 7.

3.4.2 Galvanostatic electrolysis without upper anodic cut off potential

In contrast to the electrode from run 1, the deposit formed during co-deposition of zirconium is not dense and it contains a lot of incorporated salt, which could not be removed by washing. SEM micrographs of the electrode and a detail of the interfaces Al–salt–deposit are shown in Fig. 8. The initial deposit appears to be dense and adherent, but later this gives way to a very porous deposit that is filled with salt (see Fig. 8b). The outer layer is the attached salt. Thus the co-deposition of Zr together with actinides rapidly hampers the formation of a dense An-Al alloy and results in a significant deterioration of the quality of the deposit.

EDX analyses indicated high heterogeneity of the deposit composition and presence of many salt-filled pores. The average Al/(Pu + U) ratio was determined to be 3.8 using the analyses of the deposit parts composed of an alloy. This indicates the formation of a mixture of $AnAl_3$ and $AnAl_4$ alloy. In some analyses, high Zr concentrations up to 40 wt. % were measured. The large spread in results makes a correct qualitative evaluation of total Zr content in the deposit impossible. The major phases detected by XRD analysis of the deposit are composed of (U,Pu)Al_3 alloy and KCl. Other determined compounds are $ZrAl_3$, (U,Pu)Al_4 and LiCl.

3.5 Development of concentration profile during the experiments

Concentrations of U, Pu, Zr and Gd were regularly monitored by ICP-MS analysis of the salt samples during the complete experiment. The resulting concentration profile as a function of the total passed charge is plotted in Fig. 9.

The effectiveness in the application of cut-off potentials was verified, as the concentration of gadolinium remained at its initial level and zirconium concentration was below the detection limit during the major part of the runs. An exception was detected for the run 2, where Zr was intentionally

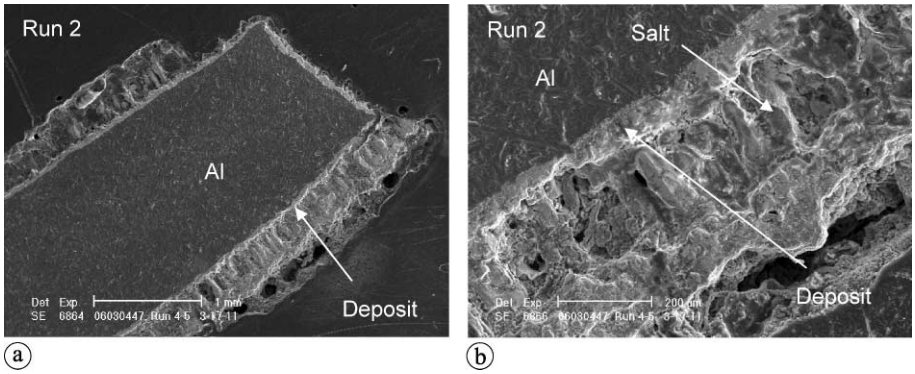

(a) (b)

Fig. 8. SEM micrographs of the electrode from run 2.

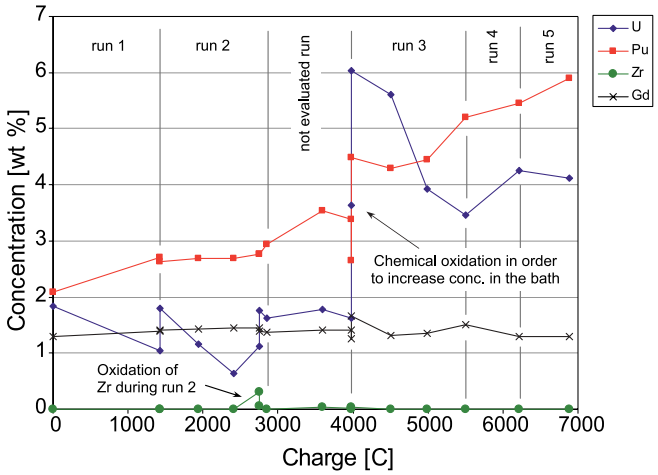

Fig. 9. Concentration profile of U, Pu, Zr and Gd in the bath during the electrorefining. The run carried out between runs 2 and 3 was not evaluated due to technical problems.

electrochemically oxidized from the U-Pu-Zr alloy together with the actinides. After this run, all dissolved zirconium was chemically reduced by the UPuZr alloy, in the anode basket, back to a concentration value below the detection limit.

The uranium concentration showed a decreasing trend during all the runs. This is explained by the congruent An dissolution of the $U_{0.71}Pu_{0.19}Zr_{0.10}$ alloy on the anodic side and the predominant deposition of U compared to Pu at the cathode (U/Pu mass ratio in the deposit is ~ 10). In addition a chemical reaction, *i.e.* reductive extraction of U^{3+} by Al from the electrode can also occur which would also lead to a decrease of the U^{3+} concentration [23]. On the other hand, the plutonium concentration gradually increased during the experiment. The concentration increase of both actinides at 4000 C was caused by intentional chemical oxidation of the alloy by addition of $BiCl_3$ according to reaction (1) in order to increase the concentration of the actinides in the bath.

4. Conclusion

The use of solid aluminium electrodes for the reprocessing of spent nuclear fuel by electrorefining in molten chlorides seems to be very advantageous. Reduced actinides form solid and dense alloys with aluminium and a very high capacity of aluminium to retain actinides has been proven in the above experiments on electrorefining of U-Pu-Zr alloy in LiCl-KCl eutectic at 450 °C. Galvanostatic and potentiostatic electrolytic techniques were applied during the experiment and almost 6000 C has been passed during the 5 evaluated runs, which were carried out under conditions suitable for a grouped separation of actinides from lanthanides. Uniform and thick deposits mainly composed of An-Al_3 alloy were obtained with a high current efficiency.

On the other hand, the presence of zirconium ions in the bath and the related zirconium co-deposition had very negative effects yielding porous and non-compact deposit. Although it is thermodynamically possible to avoid Zr dissolution from U-Pu-Zr alloy by applying an anodic cut-off potential, the complete recovery of actinides during electrorefining of An-Zr alloy fuels can not be achieved without co-dissolution of some Zr [24]. Further studies on this issue will be necessary to optimize the process.

Acknowledgment. The authors wish to thank H. Ottmar and B. Lynch for γ-spectroscopy measurements, T. Wiss for SEM analysis, C. Scheppler, S. Birck and S. v. Winckel for ICP-MS analysis as well as M. Ougier and A. Rodrigues for experimental support. This work was carried out with the European Commission financial support in the 6th framework program, under the contract FI6W-CT-2003-408854, "EUROPART".

References

1. Accelerator Driven Systems (ADS) and Fast Reactors (FR) in Advanced Nuclear Fuel Cycles – A Comparative Study. OECD/NEA (2002).
2. A Technology Roadmap for Generation IV Nuclear Energy Systems. U.S. DOE Nuclear Energy Research Advisory Committee at the Generation IV International Forum (2002).
3. Magill, J., *et al.*: Impact limits of partitioning and transmutation scenarios on radiotoxicity of actinides in radioactive waste. Nucl. Energy **42**, 263 (2003).
4. Laidler, J. J., *et al.*: Development of pyroprocessing technology. Prog. Nucl. Eng. **31**, 131 (1997).
5. Uozumi, K., *et al.*: Electrochemical behaviors of uranium and plutonium at simultaneous recoveries into liquid cadmium cathodes. J. Nucl. Mater. **325**, 34 (2004).
6. Kato, T., *et al.*: Separation behaviors of actinides from rare-earths in molten salt electrorefining using saturated liquid cadmium cathode. J. Nucl. Mater. **357**, 105 (2006).
7. Conocar, O., *et al.*: Promising pyrochemical actinide/lanthanide separation processes using aluminium. Nucl. Sci. Eng. **153**, 253 (2006).
8. Conocar, O., Douyere, N., Lacquement, J.: Extraction behavior of actinides and lanthanides in a molten fluoride/liquid aluminum system. J. Nucl. Mater. **344**, 136 (2005).
9. Serp, J., *et al.*: Electroseparation of Actinides on Solid Aluminium in LiCl-KCl Eutectic. In: GLOBAL 2003, New Orleans (2003).
10. Serp, J., *et al.*: Electroseparation of actinides from lanthanides on solid aluminum electrode in LiCl-KCl eutectic melts. J. Electrochem. Soc. **152**, C167 (2005).
11. Cassayre, L., *et al.*: Investigation of electrorefining of metallic alloy fuel onto solid Al cathodes. J. Nucl. Mater. **360**, 49 (2006).
12. Masset, P., *et al.*: Thermochemical properties of lanthanides (Ln = La,Nd) and actinides (An = U,Np,Pu,Am) in the molten LiCl-KCl eutectic. J. Nucl. Mater. **344**, 173 (2005).
13. Abousahl, S., *et al.*: Development of quantitative analytical methods for the control of actinides in pyrochemical partitioning process. Radiochim. Acta **93**, 147 (2005).
14. Masset, P., *et al.*: Electrochemistry of uranium in molten LiCl-KCl. J. Electrochem. Soc. **152**, 1109 (2005).
15. Smolenski, V., Laplace, A., Lacquement, J.: A potentiometric study of the interaction of Zr(IV) and O(II) ions in the LiCl-KCl eutectic molten salt. J. Electrochem. Soc. **151**, E302 (2004).
16. Serp, J., *et al.*: Electrochemical behaviour of plutonium ion in LiCl-KCl eutectic melts. J. Electroanal. Chem. **561**, 143 (2004).
17. Caravaca, C., *et al.*: Electrochemical behaviour of gadolinium ion in molten LiCl-KCl eutectic. J. Nucl. Mater. **360**, 25 (2007).
18. Bermejo, M. J., *et al.*: The electrochemistry of gadolinium in the LiCl-KCl on W and Al electrodes. J. Electroanal. Chem. **588**, 253 (2006).
19. Caravaca, C., De Cordoba, G.: Formation of Gd-Al Alloys Films by Molten Salt Electrochemical Process. In: EUCHEM 2006, Hammamet, Tunesia (2006).
20. Iizuka, M., Kinoshita, K., Koyama, T.: Modelling of anodic dissolution of UPuZr ternary alloy in the molten LiCl-KCl electrolyte. J. Phys. Chem. Solids **66**, 427 (2005).
21. Tougait, O., Noel, H.: Stoichiometry of UAl_4. Intermetallics **12**, 219 (2004).
22. Runnalls, O. J. C., Boucher, R. R.: Polymorphic transformations in $PuAl_3$. J. Nucl. Mater. **15**, 57 (1965).

23. Cassayre, L., *et al.*: Uranium underpotential deposition onto solid aluminium in molten LiCl-KCl eutectic. To be published (2008).

24. Ahluwalia, R. K., Hua, T. Q., Geyer, H. K.: Removal of zirconium in electrometallurgical treatment of experimental breeder reactor II spent fuel. Nucl. Technol. **133**, 103 (2001).